Red emission doublets in diamond from vacancies interacting with interstitial carbon aggregates in tunneling configurations

Andrea Zullino[1], Giorgio Benedek[2], Alberto Paleari*, Roberto Lorenzi[2]

Department of Materials Science, University of Milano-Bicocca, Via Cozzi 55, 20125, Milan, Italy

** Corresponding author: alberto.paleari@unimib.it*

[1] Present address: IGI-Istituto Gemmologico Italiano, piazza San Sepolcro 1, 20123 Milano, Italy.

2 Also at: Donostia International Physics Center (DIPC), P. Manuel de Lardizàbal 4, 20018 Donostia/San Sebastian, Spain

Abstract

Carbon vacancies in diamond are emerging as light emitting systems with outstanding properties for photonics and quantum information. The feasibility of these applications is strictly related to specific spectral and kinetic features of vacancy light emissions which, in turn, depend on the environment of the light-emitting sites. Many vacancy variants are known, from the intrinsic one to those perturbed by N and Si atoms. However, no data is available on light emissions of vacancies interacting with interstitial carbon aggregates, despite the intrinsic nature of such systems. Here we report the analysis of two emission doublets at 1.87 and 1.82 eV, and at 1.76 and 1.71 eV. The latter is systematically accompanied by the infrared signature of interstitial carbon platelets at 1365 cm^{-1} and low-energy sidebands with 8 and 16 meV splitting, tentatively assigned to tunneling modes of the split-interstitial over four equivalent configurations. Energy splitting and photon energies are consistent with vacancies at interstitial carbon structures from previous first principle calculations which find here, for the first time, an experimental confirmation in photoluminescence spectra. The data has potential to open up a new technology by controlling vacancy generation and patterning in diamond via laser writing of oriented interstitial layers.

1. Introduction

The knowledge and control of carbon vacancy sites play a crucial role in providing diamond with a technological perspective in several areas, both as a competitor of silicon in challenging applications [1] and as a potential candidate for the development of new technologies, specifically in the field of photonics [2], [3], biological imaging [4], [5], and qubit information processing [6], [7]. Charge transport and light emission properties in diamond are in fact influenced by, or even strictly dependent on charge state and electronic excitation of localized sites that are directly or indirectly related to carbon vacancies in the network. Carbon vacancies are in turn influenced by nearby lattice modifications caused by possible impurities or dopant atoms substituting for carbon – mainly nitrogen – occurring in several variants or aggregates [8]. As a result, vacancies in diamond show a number of different configurations – neutral or negatively charged – related to perturbations by nearby atoms [9]. The phenomenology arising from all vacancy-related lines and bands in the photoluminescence (PL) spectrum is quite complex, with a variety of spectral features which show peak positions ranging from ultraviolet to infrared (IR) [3], [8], and spectral linewidth from values close to the Fourier transform limit [10] to bandwidths of tens of nm, broadened by phonon interactions. Main vacancy variants arise from perturbation by nitrogen sites – studied since the '70s and actively investigated in the last decade for its stable and charge-tuneable light emission in nanodiamonds [11], [12], [13], [14]. Si substituted sites [14], [15], [16] were discovered in the '80s and found in recent years to be a unique system for the generation of single photons and single highly coherent spins for quantum information processing [3], [17], [18]. A number of other vacancy sites – included those induced by Xe implantation [19] – received anyway attention to possibly enlarge the spectral range of use of the peculiar features of vacancy light emission. No information, except for numerical calculation [20], [21], is however available on perturbations or even variants of C-vacancies nearby interstitial carbon defects or extended structural defects as platelets of interstitial carbon layers.

In the present work, we report on a PL pattern whose spectral features point to a previously unidentified variant of light-emitting sites. The new spectral pattern is accompanied by the phonon mode of interstitial carbon platelets in the IR absorption spectrum, and matches the energies calculated for electronic transitions of vacancies interacting with interstitial carbon structures. Our work indeed constitutes the first report on the optical properties of vacancies interacting with interstitial carbon sites, predicted by *ab initio* calculations [20], [21] which, up to

now, were still lacking of an experimental PL evidence. The confirmation of light-emitting variants at carbon-related nanostructures is a breakthrough in view of very recent results which prospect a novel technique of laser-induced controlled generation of layered extended defects in diamond [22], opening the way to the future creation of oriented patterns of light-emitting vacancies.

2. Materials and methods

Samples were selected out of a large set of more than one hundred type Ia diamonds (few mm^3 in size, on average), after a detailed characterization by infrared (IR) absorption measurements so as to assure an adequate sampling of diamond systems with different content of carbon platelets and other coexisting defective structures. To date, type Ia natural diamonds are in fact the systems of choice to investigate carbon platelets, which are someway related to the structural perturbation induced in natural crystals by nitrogen aggregates [23], *i.e.* the fingerprint of type Ia diamonds [8]. Furthermore, all samples were selected out of diamonds subjected to treatments of irradiation and heating (yellow diamonds with artificially modified colour [24], [25]) – able to create vacancy sites and to activate vacancy diffusion [26], so as to potentially promote vacancy trapping at extended defects. In our investigation, to get a detailed characterization of the defective state, the whole set of diamonds were analyzed by IR absorption measurements. The obtained data were then used as a basis to select samples suitable to assure adequate sampling of structures with different content of carbon platelets (see Table 1 for sample details). IR measurements in the 'one phonon' spectral region, from 1000 to 1400 cm^{-1}, were used to check and quantify the occurrence of platelets and the presence of nitrogen aggregate A and B [8]. Near IR measurements at around 5000 cm^{-1} were instead carried out to monitor H1b and H1c centres through their narrow electronic transitions [27]. Both kinds of measurements were carried out by means of a Diffuse-Reflectance Infrared Fourier-Transform (DRIFT) spectrometer with a spectral resolution of 4 cm^{-1}. DRIFT data are reported as log(1/R), where R is the relative intensity (with respect to a reference signal) of the collected diffuse signal (resulting from reflected, transmitted, and diffused signals in a wide solid angle). The log(1/R) value, in the approximation of not too a high absorption, is nearly proportional to the absorbance A, which in turn is linearly dependent on the concentration of absorbing species, according with the Lambert-Beer relationship.

Table 1. Main characteristics of the natural Type Ia diamond samples investigated in the present work.

Sample	**weight (mg)**	**colour**[a]	**relative platelet content**[b]	**N-aggregate A/B ratio**[c]
Lpc	24.6 ± 0.1	Fancy Intense Brownish Yellow	0.09 ± 0.05	≥1
Ipc-1	12.6	Fancy Greenish Yellow	0.32	0.7 ± 0.05
Ipc-2	12.8	Fancy Intense Greenish Yellow	0.24	0.8
Ipc-3	14.4	Fancy Greenish Yellow	0.19	1.4
Hpc	69.2	Fancy Intense Greenish Yellow	1.00	NA

aGemological Institute of America (GIA) colour grading scale.

bCalculated from the integrated IR band in the spectral region 1350-1400 cm^{-1} normalized to the Hpc value.

cRatio between intensity sum at 1210 and 1282 cm^{-1} and at 1170 and 1331 cm^{-1} in the IR spectrum (NA = not available).

PL measurements were carried out exciting at two wavelengths by means of Ar laser at 488 nm or HeNe laser at 633 nm with beam density power of the order of 10^{-1} W/mm^2, shuttered at a frequency of 1 Hz. The light signal was collected by a charge-coupled-device after dispersing the signal by a polychromator with a final resolution of 4×10^{-4} eV. Before analysis, all spectra were normalized at the intensity of the diamond Raman mode at 1332 cm^{-1}. PL peak intensities were determined after subtraction of the background, with an uncertainty of few % at most. Measurements at different temperature, in the range between 77 and 300 K, were carried out by means of a cryostat working with liquid nitrogen flux and a programmable heater, with a final thermal stabilization within ±2 K.

3. Results and discussion

3.1. Nitrogen aggregates and carbon platelets

In Fig. 1a we report IR spectra of samples representative of the variety of platelet-containing type Ia diamonds. Within the entire spectral range from 400 to 6000 cm^{-1} we register all the main expected features of this class of materials, with differences from sample to sample as underlined below. At energy comprised between about 1000 and 1400 cm^{-1} (see Fig. 1b), we find strong absorption structures from nitrogen aggregates and interstitial carbon platelets. Specifically, at 1210 and 1282 cm^{-1} the spectra show the absorption bands caused by A aggregates – i.e. defect complexes describable as N=N pairs substituting for pairs of C atoms – and at 1170 and 1331 cm^{-1} the features of B aggregates, consisting of four nitrogen atoms substituting for carbon around a C vacancy site. We do not detect the absorption bands at 1344 and 1110 cm^{-1} related to isolated substitutional N atoms - C defects. At higher energy, at around 1360-1370 cm^{-1}, we register the phonon mode of interstitial carbon platelets, whose spectral position shows some variation, slightly depending on the platelet size (see Fig. 1c) – the larger the platelet, the smaller the phonon energy [21]. The 1000-1400 cm^{-1} region is where the main differences among samples occur, reflecting different content of A and B aggregates and interstitial carbon platelets. The five selected samples comprise a high-platelet-content system (Hpc sample), three intermediate-platelet-content systems (Ipc samples) with different ratio between A and B aggregates (Ipc-3, Ipc-2 and Ipc-1 samples, from largest to smallest A/B ratio), and a reference system with very low content of platelets (Lpc sample). Referring to the type classification system of diamond, the analyzed samples can be classified as type IaA, IaAB (with A > B, A < B, and A ≈ B) and IaB.

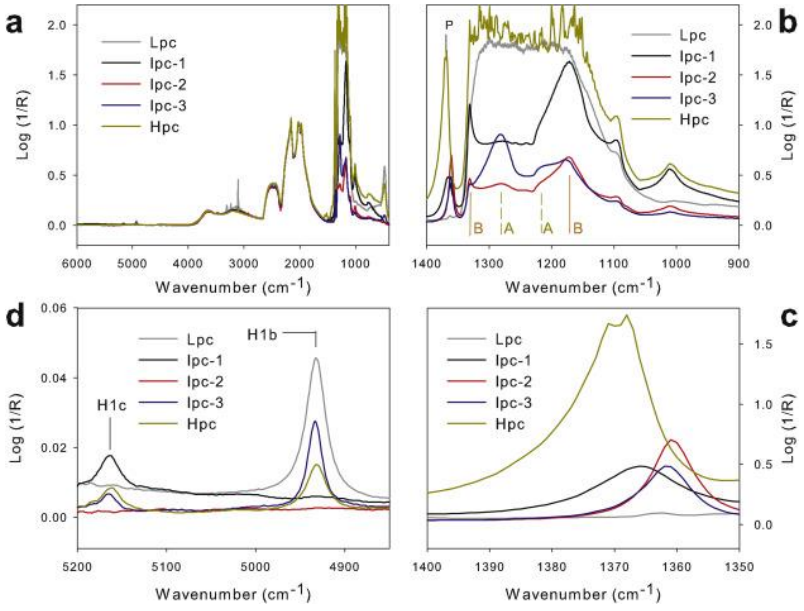

Fig. 1. Infrared absorption analysis. (a) Full range normalized DRIFT spectra of the investigated samples, labelled as in the text: Hpc (high platelet content), Ipc-1,2,3 (intermediate platelet content with increasing ratio - from 1 to 3 - between A and B aggregates), and Lpc (low platelet content). (b) 'One phonon' region spectra with spectral positions of modes caused by carbon platelets (P) and A and B nitrogen aggregates. (c) Spectral region of carbon platelet mode. (d) near-IR electronic transitions of H1b and H1c centres at 4932 and 5162 cm^{-1}.

The spectral position of the platelet mode ranges from 1370 to 1360 cm^{-1}, reflecting differences in the mean platelet size [21]. In Fig. 1d, we report the details of the spectral region of the electronic transitions H1b e H1c at 4932 and 5162 cm^{-1}, respectively. Such narrow peaks are not definitely ascribed to specific defects yet. However, H1b and H1c are someway related to the evolution of A and B aggregates, respectively, after irradiation and heating treatments [8]. The spectra in Fig. 1d in fact register low intensity of H1b peak in samples with weak contributions of A aggregates in the IR spectrum in the region 1000-1400 cm^{-1} (Fig. 1b). In summary, the set of selected samples turns out to be representative of the main varieties of platelet-containing diamonds, comprising quite different platelet contents and, at comparable platelet content, different amount of A and B nitrogen aggregates and the related H1b and H1c centres.

3.2. Doublets in the photoluminescence spectra

We report in Fig. 2 PL spectra collected at 77 K exciting at 488 nm (Fig. 2a) and 633 nm (Fig. 2b). The spectra in Fig. 2a show much of the known phenomenology of nitrogen-containing Type I diamonds. Specifically, we register intense peaks at 496 and 503 nm (with structured phonon sidebands) from H3 and H4 centres – attributed to vacancies trapped at A and B nitrogen aggregates – and the well-known NV^0 and NV^- zero phonon lines and their related phonon sideband signals at 575 nm and 637 nm, respectively. Additional minor peaks (undetectable at room temperature) lie in the 650–750 nm red region, outside the set of main spectral structures which already received an attribution. We obtain much better evidence of such undefined peaks in the spectra excited at 633 nm (Fig. 2b), since a large part of the decay processes excited by 488 nm radiation are removed. The lack of all the main emissions of Type I diamonds allows us to highlight features not previously analyzed in detail. In fact, looking at Fig. 2b, main features above the continuum is a pattern consisting of two doublets of spectral structures – each one split in two

lines at low temperature – with sample-dependent ratio between the intensities of the two doublets. From shorter wavelength, the first doublet (hereafter called D_a doublet) shows main peaks at 662 and 681 nm, whereas main peaks of the second one (hereafter called D_b doublet) fall at 704 and 724 nm. Grouping the lines in two doublets comes from the comparison of patterns of different samples. In fact, the peaks at 704 and 724 nm are always found together (as we verified in the extended set of more than one hundred samples), as well as the peaks at 662 and 681 nm. By contrast, the D_a doublet can occur without D_b and vice versa, as exemplified in the spectra of samples Lpc and Ipc-1 in Fig. 2b, respectively. Interestingly, by comparing PL spectra of Fig. 2b and IR data of Fig. 1, we notice that D_b is not detected in the platelet-free sample. Indeed, considering the whole set of analyzed samples, we find that D_b is always accompanied by the IR signal of platelet mode at about 1360 cm^{-1}. As regards D_a, its intensity is low or even undetectable in samples where the signal of A aggregates is weak (samples Ipc-1 and Ipc-2). However, since platelets and nitrogen aggregates are not *per se* light-emitting systems, but only when they accommodate nearby active sites like vacancies, no direct quantitative relationship is registered nor is it expected between the intensity of PL doublets and the IR absorption ascribed to platelets or nitrogen aggregates. To have suggestions on the defect configuration responsible for D_a and D_b, we analyze here below the details of their transition energies, energy splitting and temperature dependence.

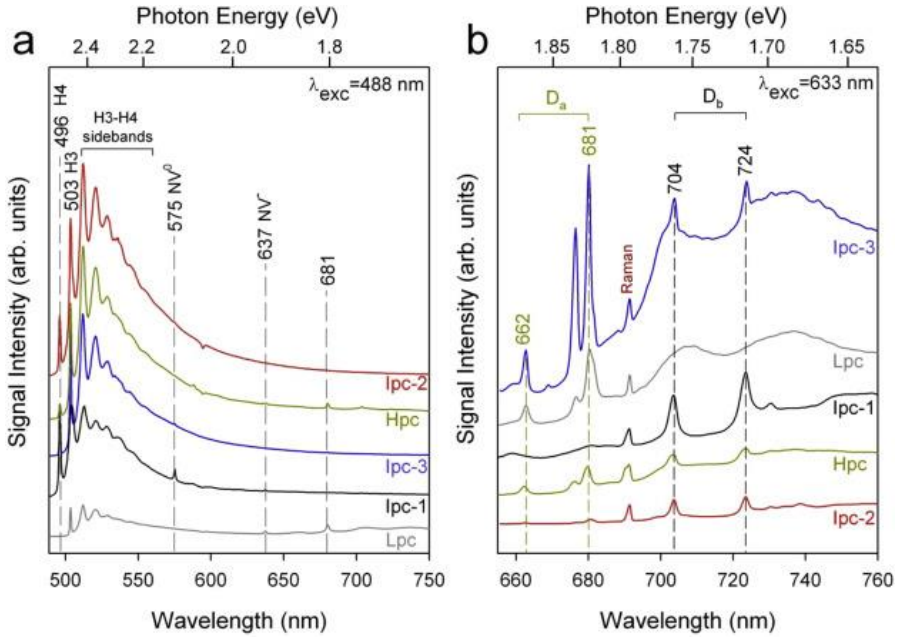

Fig. 2. Photoluminescence response. Spectra collected at 77 K exciting at (a) 488 nm and (b) 633 nm. In (a) the spectral position of the main light emissions are indicated (in nm) together with the label of the responsible defect. In (b) the D_a and D_b doublets are

indicated, as well as the Raman mode of diamond. The spectra are vertically shifted for clarity.

3.3. Temperature-dependent intensity changes in D_a and D_b doublets

In Fig. 3, we report PL spectra which exemplify the temperature dependence of the observed doublets in three representative systems (Hpc, Ipc-1, and Lpc) with very different value of the ratio between D_a and D_b doublets. The spectra in Fig. 3 underline the strong difference between the influence of temperature on the relative intensities of the two lines within each doublet in D_a and D_b signal. In fact, the D_b lines keep their intensity ratio almost constant with the temperature and of the same order of magnitude in different samples (see Fig. 3a–c). Single emissions at approximately the same energy of the D_b lines were reported in the literature [8], [28], [29], but detected at low temperature only and, importantly, never associated to each other in a doublet of lines.

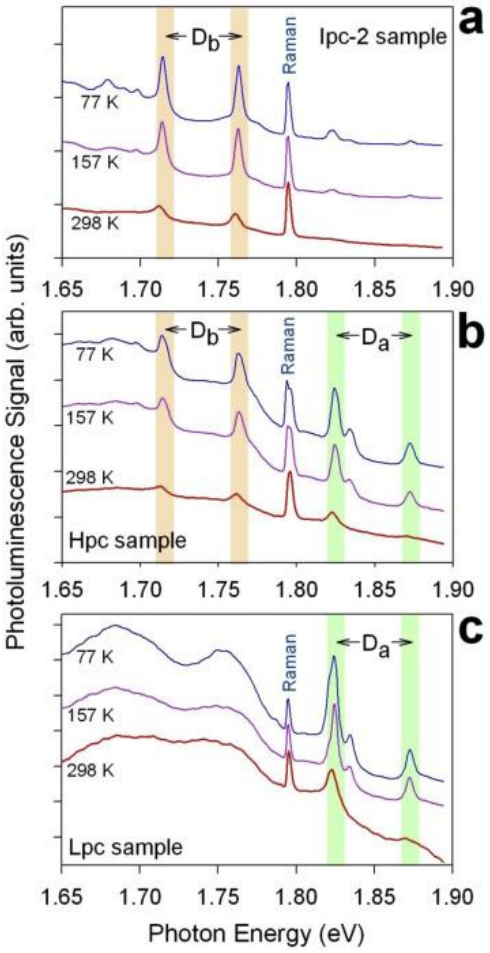

Fig. 3. D_a and D_b light emissions vs temperature. PL spectra excited at 633 nm at three different temperatures in representative diamond samples with (a) D_b intensity much higher than D_a, (b) comparable D_a and D_b intensities, (c) D_a doublet without D_b. All spectra

are normalized with respect to the intensity of the Raman line of diamond (equal to the scale unit of the y-axis) and vertically shifted for clarity.

The emissions in the D_a doublet, differently from the D_b doublet, show a strong change of intensity ratio. The high-energy line at 1.87 eV (662 nm) decreases with increasing the temperature and turns out undetectable at 298 K (Fig. 3a–c). As a result, the low energy line of the D_a doublet at 1.82 eV (681 nm) appears as a single line at room temperature. Interestingly, its peak wavelength falls just in the spectral position of a previously reported emission [30] which however, at the best of our knowledge, has not been associated to a doublet of lines nor has it received an attribution yet.

The different temperature dependence of D_a and D_b intensity is quantified in Fig. 4 in the case of two samples showing both doublets (Icp-2 and Icp-3 samples in Fig. 4a and b, respectively). We notice differences in the relative intensity changes of the two D_a lines. By contrast, D_b lines show instead similar thermal behaviour in all samples, and the intensity ratio between 704 and 724 nm peaks (1.76 and 1.71 eV, respectively) turns out quite independent of the temperature (see upper side of Fig. 4a and b).

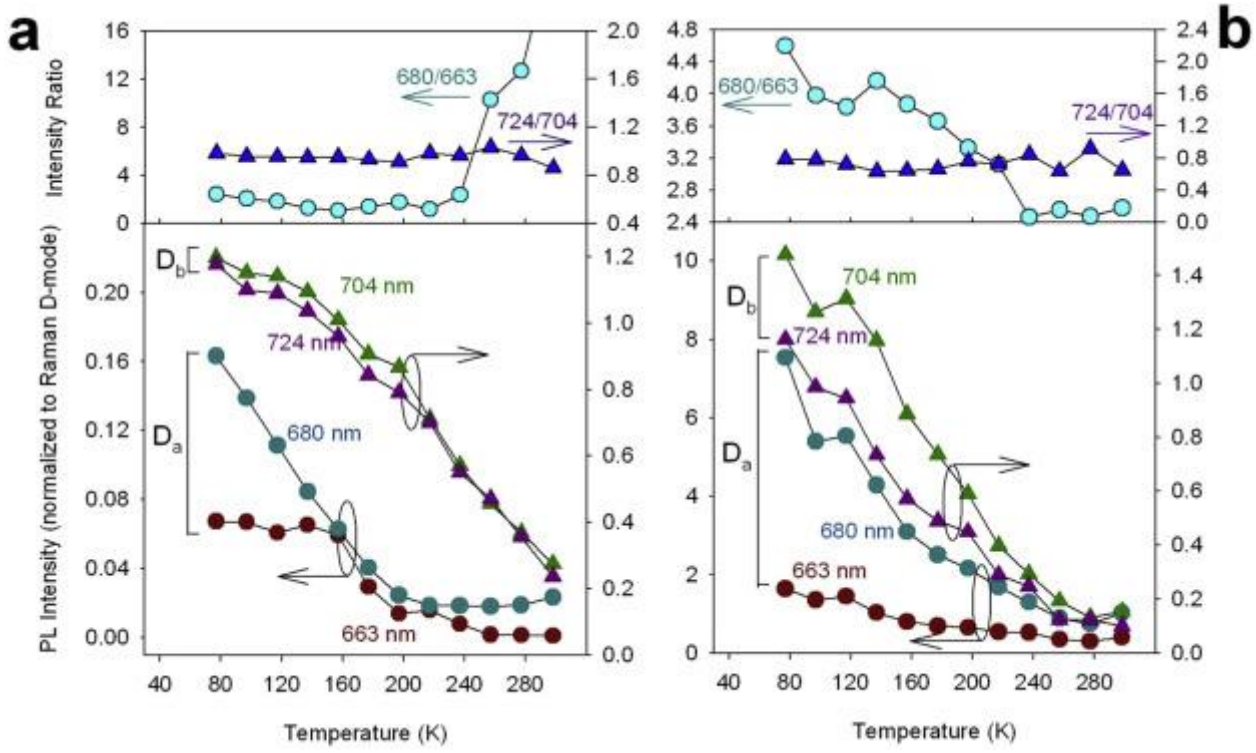

Fig. 4. Temperature dependence of D_a and D_b line intensity. (a) Intensity (lower part) and intensity ratio (upper part) of D_a doublet lines at 662 and 681 nm (circles) and D_b doublet

lines at 704 and 724 nm (triangles) at three temperatures in sample Ipc-2 with intermediate platelet content and intermediate ratio between A and B aggregates. (b) the same as in (a) in sample Ipc-3 with higher ratio between A and B aggregates.

3.4. Satellites and replicas in D_a and D_b doublets

Minor peaks – almost undetectable at room temperature but easily observed at low temperature – accompany almost all the main emissions. Specifically, looking at Fig. 5, we notice that both the D_a lines (Fig. 5a), as well as the D_b components (Fig. 5b), show a minor satellite about 10 meV higher in energy. Similar high-energy satellites, with comparable splitting from the main line, were found in other absorption and emission lines of vacancy centres in diamond, specifically in the spectra of negatively charged vacancy and of the neutral vacancy [31], [32]. In those cases, the splitting turns out to be ascribable to Jahn-Teller effect on the involved states. Furthermore, the two D_b lines show low energy replicas spaced by about 8–10 meV (more evident in the low energy 724 nm line at 1.71 eV), which highlight a possible coupling to some low-energy excitation of energy of about 65–80 cm^{-1}, considerably lower than all typical diamond phonons. This is discussed below. Comparing different diamond samples (see Fig. 3), we notice that the narrower the D_b lines, the clearer are the replicas. Instead, replicas are not observed in the sample Lpc in which the D_b doublet is not detected at all. Changing the temperature, not only the spectral position, but also the intensity of all minor signals – high-energy satellites and low-energy replicas – follows the intensity of the main D_b and D_a lines.

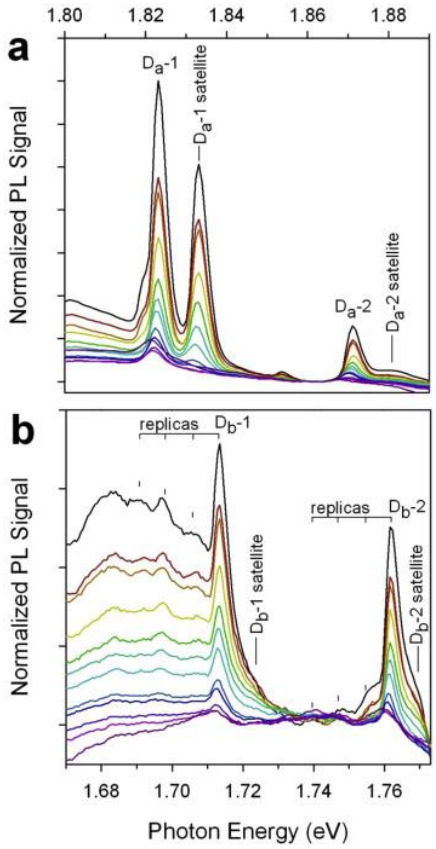

Fig. 5. Satellites and replicas of D_a and D_b lines at different temperature. PL spectra in IPC-3 sample excited at 633 nm and collected at different temperature from 77 K (most intense spectrum) to 298 K (less intense spectrum) at step of 20 K, in the spectral region of (a) D_a doublet and (b) D_b doublet. The average replica spacing is 7.5 meV for D_b-1 and 7.3 meV for D_b-2.

We report in Fig. 6a the spectral position of all the detected peaks in the temperature range from 77 to 300 K in the case of sample Ipc-3. It is worth noting, looking at Fig. 6a, that the energy splitting of D_a and D_b doublets are almost equal, about 48 meV. Furthermore, we register a small shift – about 3 meV – of all spectral structures, major and minor lines, to lower energy at increasing temperature. The order of magnitude of the energy shift δE, reported in Fig. 6b for the main four lines of D_a and D_b doublets, is consistent with that observed both in NV and SiV vacancy centres (which ranges from 2 to 3 meV) [33], [34], [35], [36]. The temperature dependence of the spectral position follows the expression $\delta E = \mu T^2 - \nu T^4$, similarly to other data on vacancy light-emitting sites [33], [34], [35], [36]. We find $\mu = 9.0 \times 10^{-9}$ eV/K^2 and $\nu = 3.9 \times 10^{-13}$ eV/K^4 for D_a lines, while in D_b lines we obtain $\mu = -2.2 \times 10^{-8}$ eV/K^2 and $\nu = 5.6 \times 10^{-14}$ eV/K^4. In SiV and NV sites, for comparison, ν turns out 1.2×10^{-13} and 3.1×10^{-13} eV/K^4, respectively, with μ values equal to 2.5×10^{-8} and 9.9×10^{-9} eV/K^2, respectively.

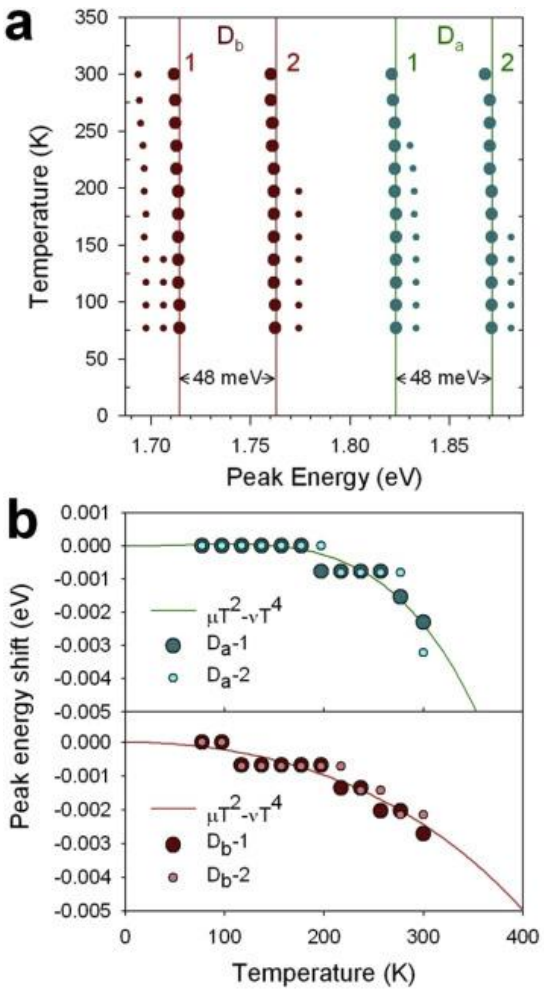

Fig. 6. Temperature dependence of spectral positions. (a) Spectral position vs temperature of major (big marks) and minor (small marks) lines of D_a and D_b doublets. (b) Temperature-induced spectral shift (referred to 77 K position) of low energy (large circles) and high energy (small circles) lines of D_a doublet (upper part) and D_b doublet (lower part). Curves are fits with μT^2-νT^4 dependence of D_a (green) and D_b (red) lines.

The μ and *v* values we estimate in D_a are quite similar to those calculated for NV sites. By contrast, the thermal shift of the D_b lines indicate a μ/*v* ratio significantly greater, with a contribution of the T^2 term larger than in all other vacancy centres. We notice that the T^4 term arises from the combined effects of local stress by lattice expansion (varying as T^4 [35], [37]) and electron-phonon quadratic coupling with hard phonon modes mainly (whose term varies as T^4 as well [33], [35], [38]). By contrast, contributions with T^2 dependence are the result of a strong softening of phonon modes in the excited state [33]. Therefore, our data points to an important role of soft modes in the electronic transitions responsible for the D_b doublet.

It is worth noting, as regards the electron-phonon coupling, that the D_b component at 1.71 eV displays a sideband, mainly detectable in the low energy side (Fig. 3, Fig. 5). Looking at the 1.71 eV line of the D_b doublet and its sideband, we can highlight some relevant facts. First, the spacing of the low-energy replicas (of a few meV) is sensibly narrower than that encountered in the majority of light-emitting defects in diamond [38]. Second, the energy spacing is sample dependent in the investigated samples (see spectra in Fig. 2, Fig. 3). Third, besides such a distribution of energy spacing from sample to sample, we also observe a sample dependent broadening of the replicas as well as of the main line at 1.71 eV. Starting from these facts, we notice that extended defects of interstitial carbon layers can constitute a source of sample-dependent electron-phonon interactions, since they are aggregations with size distribution largely varying from sample to sample, provided that the size differences from sample to sample are enough to cause detectable spectral changes. To verify this possibility, we reconsider the evidences of carbon platelets in the IR spectra in Fig. 1c, looking at the differences of bandwidth among the samples.

We report in Fig. 7a the relationship we have found between the 724 nm line broadening at 77 K and the bandwidth of the platelet phonon mode at 1360-1370 cm^{-1} in the IR spectrum. The correlation suggests that interstitial structures play a role in the D_b doublet. Furthermore, since the broadening of the IR platelet band turns out to be a measure of the platelet size distribution (because the platelet size determines the phonon mode energy [21]), we expect that also the IR platelet band position (dependent on the mean size of platelets [21]) must be related to some features of the low-energy excitation sideband of the 1.71 eV line of the D_b doublet. In Fig. 7b, we notice that the data of energy spacing between replicas in the 1.71 eV sideband of different samples (from the analysis of spectra in Fig. 5) show differences that follow the shift of spectral position of the platelet phonon mode (from Fig. 1c). In summary, while the number of experimental points in Fig. 7a and b, separately, is not so large to definitely confirm a correlation, the two sets of data, together, give an important hint of an intimate interaction of D_b light-emitting sites with interstitial carbon structures. For this reason we have looked for additional evidences comparing our data with previous *ab initio* calculations on vacancies at interstitial aggregates and with original theoretical estimation of sideband contributions from interactions with interstitials. In fact, the excitation energies in the D_b sideband are completely different from the platelet phonon mode at 1360 cm^{-1}. They evidence the involvement of low energy excitations in the hard covalent structure of diamond.

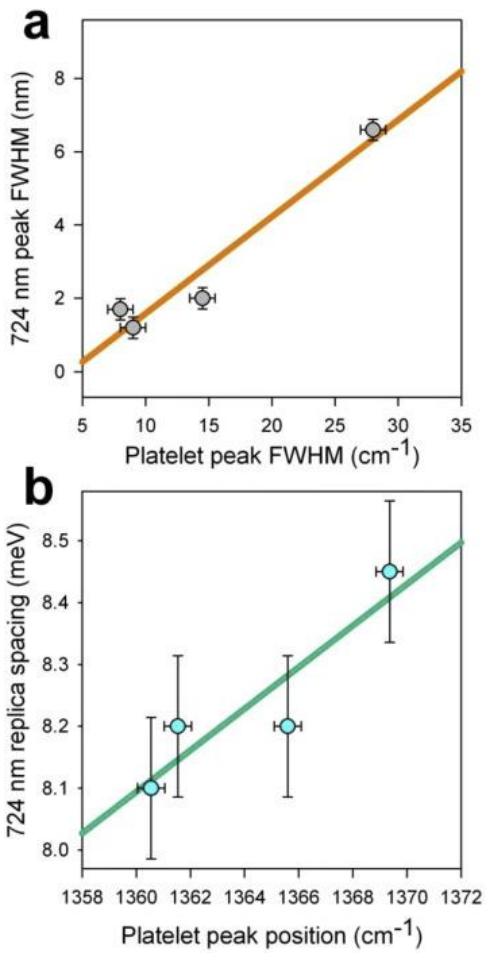

Fig. 7. Relationship between D_b doublet and platelet IR band. (a) Full width at half maximum (FWHM) of the 724 nm (1.71 eV) peak of D_b doublet vs. FWHM of the platelet phonon band at 1360-1370 cm^{-1} in the investigated sample set. (b) Spacing of low-energy excitation replicas in the 724 nm D_b sidebands vs. spectral position of the platelet band.

The low-energy Raman spectrum we collected in platelet-rich samples indeed indicates the occurrence of soft modes with energy of about 75 and 150 cm^{-1} (Fig. 8). Interestingly, spectral position and energy distribution of the two Raman structures are approximately consistent with energy spacing and linewidth of D_b sideband replicas, possibly ascribable to the superposition of two series with energy spacing one the double of the other.

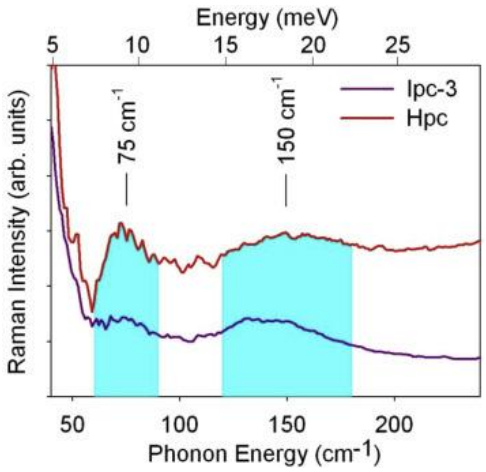

Fig. 8. Low energy Raman spectrum of representative diamond samples. Dashed areas indicate the soft energy modes.

3.5. Comparison with calculations and models

The articulated scheme of spectral energies and temperature-dependent intensities reported in Fig. 4, Fig. 6 provides a first insight into the energy structure of the light emitting centres responsible for the D_a and D_b doublets. Specifically, the change of intensity ratio in the D_a doublet as a function of the temperature indicates that the doublet splitting probably regards the excited states. By contrast, the constant intensity ratio within the D_b doublet is consistent with an energy splitting ascribable to the final states of the responsible transitions. Energy splitting and satellites of D_a and D_b signals are schematically summarized in Fig. 9, taking into account for spectral positions and temperature dependences of intensity ratio.

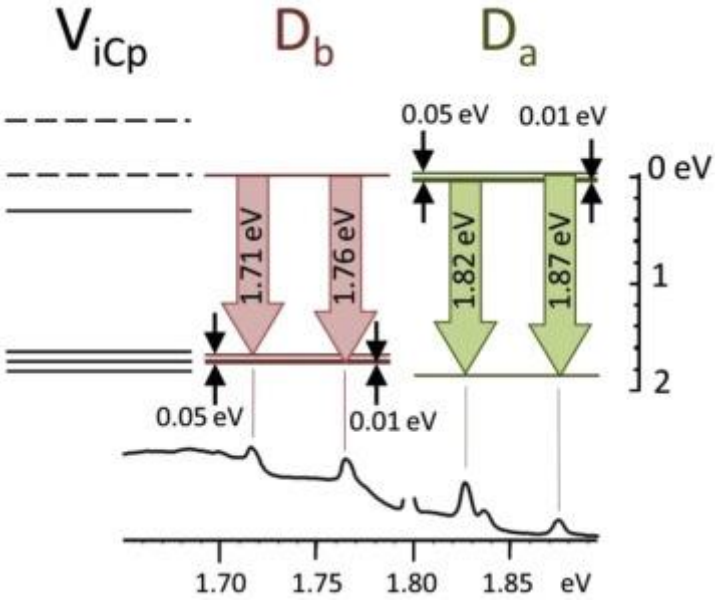

Fig. 9. Energy level scheme of doublet-emitting centres D_a and D_b. Schematic energy level structure of the levels responsible for D_a (green lines) and D_b (red lines) PL doublets (reproduced in a representative spectrum at the bottom of the figure), including ground or excited state splitting accounting for the observed temperature dependence of intensity ratio within each doublet, as well as for minor satellites. For comparison, black lines under the labels V_{iCp} schematically report occupied (full lines) and empty (dashed lines) localized energy levels (restricted to the energy region of localized levels at the top of the valence band and in the gap) from previous calculations of Kohn-Sham level schemes for a vacancy in interstitial carbon platelet (V_{iCp}) [21].

We notice that the energy spacing of the D_b doublet is consistent with the energy level scheme of a vacancy site at interstitial carbon platelets as it was obtained from first principle calculations [21], as we report for comparison in Fig. 9. In fact, vacancy sites at interstitial platelets would account for the relationship between D_b PL and platelet IR features (Fig. 7). Furthermore, the ladder-like interstitials structure in a platelet – following the proposal by Goss et al. [21] and based on the Humble structure [39] – can be the source of local soft modes responsible for both the spectral shift of D_b lines with the temperature (Fig. 6) and the low energy Raman spectrum in Fig. 8, which is in turn consistent with the D_b structure sidebands (Fig. 3, Fig. 5). In fact, the occurrence of vacancies - together with N atoms - locally preventing the full bond-reconstruction can stabilize 2C=C-C=2C structures of pair of under-coordinated carbon sites (Fig. 10a).

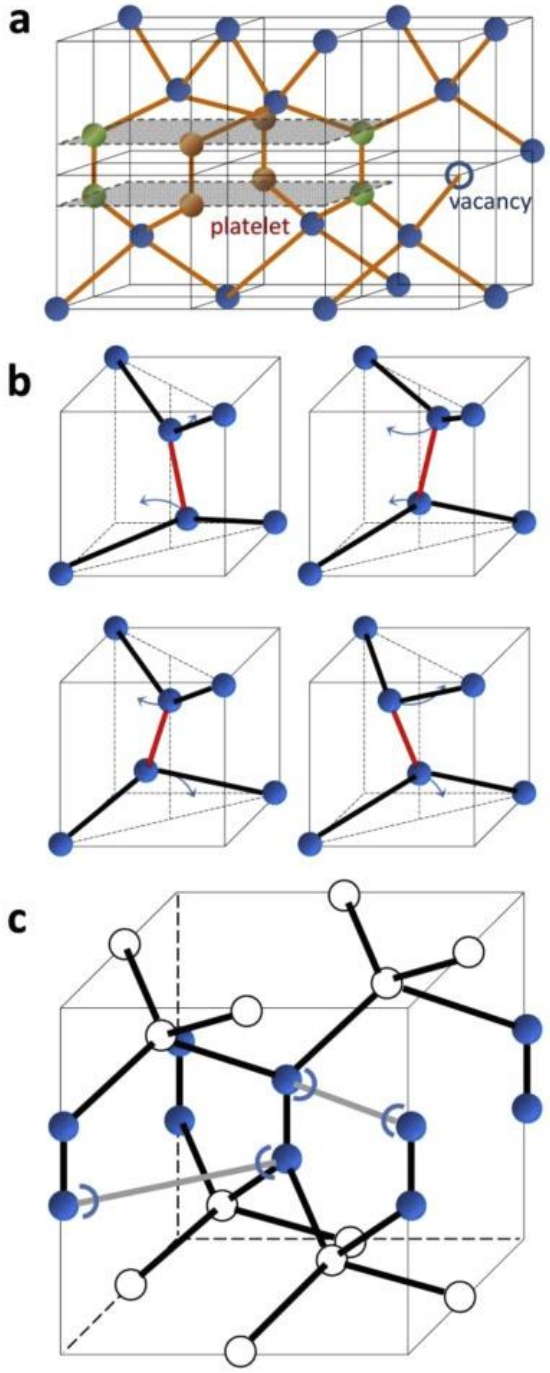

Fig. 10. Platelet structure and low energy excitations. (a) Portion of diamond structure (C-sites in blue) modified by interstitial carbon (green balls) and nitrogen (brown balls) atoms in a configuration analogous to Goss and Humble platelet models [21], [39], also depicting a platelet-related vacancy site (empty circle). (b) Sketch of an almost stretching-free vibration of three-fold coordinated atom pairs in a platelet: the two C atoms oscillate via bending vibration among four equilibrium positions. The bond between atoms (in red) oscillates with a vanishing stretching contribution. (c) Portion of a platelet in the diamond

structure, showing the possible bonding saturation (in grey) of the interstitial atoms, with indication of the displacements towards the equilibrium positions.

These structure can in turn give phonon modes at relatively low energy thanks to almost pure bending vibrations of the pair of three-fold coordinated = C– sites (as sketched in Fig. 10b,c).
As regards the D_a doublet, which does not show a systematic correlation with the occurrence of platelets, we register a partial matching with energy spacing of other species of interstitial carbon defects, as the [001]-oriented split interstitial $I_1^{<001>}$ or some forms of the di-interstitial I_2 [20]. Actually, the reported spectral data alone are not enough to support such an attribution, and both $I_1^{<001>}$ and I_2 were associated to an optical activity [20] which we do not observe. However, our results on the D_a doublet suggest the possibility of some additional variants of vacancy at interstitial carbon aggregates which might be checked by future computational studies.

3.6. A model for the low-energy excitations

Fig. 10b illustrates a rotational motion of the split-interstitial through four different equivalent oblique positions. It is however readily seen that the rotation is hindered by a potential barrier between any adjacent equilibrium positions whose height ΔV is much larger that the observed replica spacing. Thus the low-energy excitations of D_a and D_b sidebands and low-energy Raman spectrum are more likely to be tunneling modes, as proposed by Goss et al. [20], Davies et al. [40] and Smith et al. [41]. For the four-well potential of D_{2d} symmetry and tunneling only between adjacent minima there are four tunneling states: one for a totally symmetric state A_1 of energy -2Δε, two degenerate states E of energy 0 (taken as a reference) and one state B_1 of energy 2Δε, where Δε is the energy splitting for the corresponding double well potential.
The potential of one of the two split-interstitial atoms as a function of the displacement *u* from his equilibrium position towards its vertical position (the barrier maximum) can be written as(1)ΔV(u)=(Kbr02+18Ksu2)(1d2+2r2)u2where K_s = 24.28 eV/Å^2 and the K_b = 2.236 eV/Å^2 are the two-body nearest-neighbor stretching and three-body angle bending force constants of the valence-force-field model for diamond [42], respectively, r_0 = 1.545 Å is the interatomic distance in diamond, *d* = 1.26 Å the split-interstitial interatomic distance as obtained from *ab-initio* calculations [43] and *r* = 1.29 Å the corresponding distance of a split-interstitial atom from its lattice nearest neighbor. The use of the diamond force constants for the split-interstitial system with severely distorted bond lengths and angles corresponds to assuming a harmonic

approximation. Thus the presence of a u^4 term in Eq. (1) would be inconsistent with the model. However for u = 0.08 Å [40], [41] the u^4 stretching term is completely negligible and $\Delta V(u)=(9.794\ \text{eV/Å}^2)u^2 = 62.68$ meV. The ground-state tunnel level splitting for intersecting parabolic potentials can be approximated by Ref. [44].(2)2Δε=2ℏωπe−2ΔV(u)/ℏωwhere $\hbar\omega$ is the rocking oscillation energy of the split-interstitial in the parabolic well. This can be estimated by observing that the two eigenvectors for in-phase and anti-phase motion of the two atoms have the same energy, and so is for their sum or difference, i.e., for the oscillation of any of the split-interstitial atoms with the other at rest. The energy of this mode is approximately $\hbar\omega \approx \hbar(6\ k_b/M)^{1/2} = 67.94$ meV, where M is the carbon atom mass, This phonon energy is of the order of, but smaller than the energy of the zone-boundary transverse acoustic phonon of diamond in the 〈100〉 direction (98 meV [42]). With the above values one obtains $2\Delta\varepsilon$ = 6.84 meV. The value of $2\Delta\varepsilon$ has however an exponential dependence on u^2: *e.g.*, a slightly smaller displacement of u = 0.075 Å yields $2\Delta\varepsilon$ = 8.54 meV. The latter value is in good agreement with the observed Raman mode of 75 cm^{-1} (9.3 meV), while the former agrees well with the PL replica spacings of 7.5 and 7.3 meV for the D_b-1 and D_b-2 lines, respectively. The PL replica spacing is that for the tunneling when the electron system is in the initial excited state and is therefore expected to be smaller than the ground-state spacing observed with Raman. Thus a value of the order of 0.07 Å appears to be more consistent with the ground-state tunneling dynamics of the split-interstitial. On the other hand the double-well model discussed by Davies et al. [40] gives a ground-state splitting of 6 meV for u = 0.08 Å. Thus the present analysis based on a four-well potential is consistent with observation as well as with the previous studies.

We also notice that the PL sideband shows a prominence of the even-order replicas. Assuming that all tunneling transitions have the same coupling to the PL process, this may simply reflect the fact that the 2nd, 4th … order replicas receive, in addition to the contributions of 2,4, …tunneling transitions $A_1 \rightarrow E$ or $E \rightarrow B_1$ of energy $2\Delta\varepsilon$, also those of 1,2…transitions $A_1 \rightarrow B_1$ of energy $4\Delta\varepsilon$. Since tunnel excitations in a single split-interstitial cannot exceed the total energy of $4\Delta\varepsilon$, the apparent truncation of the sideband beyond the 4^{th}-order replica suggests that no more than two split-interstitials are involved in a single PL transition. As regards Raman scattering, all three possible tunnel transitions are Raman active, with the peak at 150 cm^{-1} receiving both the one-excitation $A_1 \rightarrow B_1$ and the two-excitation contributions from the combinations of $A_1 \rightarrow E$ and $E \rightarrow B_1$.

4. Conclusions

Our work highlights two new PL doublets in the red spectral region of type Ia diamonds. These doublets are observed for the first time, among several known spectral structures arising from radiation-induced vacancies which thermally migrate towards different kinds of defects and aggregates. The small concentration of the responsible optically active point defects interacting with macroscopic platelets, as well as the unusual excitation conditions for making these red emissions detectable over very efficient radiative decay channels at higher energy, have prevented until now their identification and analysis. The new phenomenology includes the D_b doublet of lines at 1.71 and 1.76 eV which shows to be correlated with the spectral features of the IR band of interstitial carbon platelet phonon mode at 1360-1370 cm^{-1}. The structure of phonon replicas in the transition sideband gives evidence of low energy excitation modes, about 75 and 150 cm^{-1} in energy, which unveil unknown details of the platelet energy structure which are potentially useful to refine the description of such aggregations. Specifically, we have found that the experimental data matches the excitations energy expected for a tunneling process between equivalent configuration of interstitial sites. Our results constitutes an unprecedented evidence of possible occurrence of light emission from vacancies at interstitial extended defects.

The present results open also the way to a number of possible applications which are related to the role of extended defects as trapping sites for light emitting vacancies. On the one hand, in natural Type Ia diamonds, the light emission of the new variant of vacancies, which are generated and mobilized towards interstitial platelets by irradiation and heating processes, might constitute a new probe of artificial treatments in gemmological diagnostics. On the other hand, in synthetic CVD diamonds, the controlled formation of extended defects by laser writing (as recently reported [22]) might be used to create selectively shaped collectors of light emitting platelet-interacting vacancies (according to the present finding), generated and mobilized by suitable technological processes. The possibility, in principle, of creating interstitial-interacting vacancies in synthetic material would indeed permit to build up oriented patterns of light-emitting vacancies as block units of complex diamond-based light emitting integrated optical systems, with a potential for photonics, bioimaging, and sensors.

Acknowledgements

We acknowledge the support and collaboration of the IGI-Istituto Gemmologico Italiano, Italy, under Contract no. 0013885/15 and 2017-COMM25-0034. The research leading to these results has also received funding from the Cariplo Foundation, Italy, under Project no. 2012-0920.

References

[1] R.S. Balmer, J.R. Brandon, S.L. Clewes, H.K. Dhillon, J.M. Dodson, I. Friel, *et al.*
Chemical vapour deposition synthetic diamond: materials, technology and applications
J. Phys. Condens. Matter, 21 (2009), p. 364221

[2] N. Mizuochi, T. Makino, H. Kato, D. Takeuchi, M. Ogura, H. Okushi, *et al.*
Electrically driven single-photon source at room temperature in diamond
Nat. Phot., 6 (2012), pp. 299-303

[3] I. Aharonovich, E. Neu
Diamond nanophotonics
Adv. Opt. Mater., 2 (2014), pp. 911-928

[4] Yi-Ren Chang, Hsu-Yang Lee, Kowa Chen, Chun-Chieh Chang, Dung-Sheng Tsai, Chi-Cheng Fu, *et al.*
Mass production and dynamic imaging of fluorescent nanodiamonds
Nat. Nanotechnol., 3 (2008), pp. 284-288

[5] V. Petráková, A. Taylor, I. Kratochvílová, F. Fendrych, J. Vacík, J. Kučka, *et al.*
Luminescence of nanodiamond driven by atomic functionalization: towards novel detection principles
Adv. Funct. Mater., 22 (2012), pp. 812-819

[6] C.G. Yale, F.J. Heremans, B.B. Zhou, A. Auer, G. Burkard, D.D. Awschalom
Optical manipulation of the Berry phase in a solid-state spin qubit
Nat. Phot., 10 (2016), pp. 184-190

[7] W.B. Gao, A. Imamoglu, H. Bernien, R. Hanson
Coherent manipulation, measurement and entanglement of individual solid-state spins using optical fields
Nat. Phot., 9 (2015), pp. 363-373

[8] A.M. Zaitsev

Optical Properties of Diamond

Springer, Berlin (2001)

[9] Gordon Davies, Simon C. Lawson, Alan T. Collins, Alison Mainwood, Sarah J. Sharp

Vacancy-related centers in diamond

Phys. Rev. B, 46 (1992), pp. 13157-13170

[10] L.J. Rogers, K.D. Jahnke, T. Teraji, L. Marseglia, C. Müller, B. Naydenov, *et al.*

Multiple intrinsically identical single-photon emitters in the solid state

Nat. Commun., 5 (2014), p. 4739

[11] C.D. Clark, C.A. Norris

Photoluminescence associated with the 1.673, 1.944 and 2.498 eV centres in diamond

J. Phys. C, 4 (1971), pp. 2223-2229

[12] G. Davies, M.F. Hamer

Optical studies of the 1.945 eV vibronic band in diamond

Proc. R. Soc. Lond. A, 348 (1976), pp. 285-298

[13] V. Petrakova, I. Rehor, J. Stursa, M. Ledvina, M. Nesladeka, P. Cigler

Charge-sensitive fluorescent nanosensors created from nanodiamonds

Nanoscale, 7 (2015), pp. 12307-12311

[14] J.P. Goss, R. Jones, S.J. Breuer, P.R. Briddon, S. Öberg

The twelve-line 1.682 eV luminescence center in diamond and the vacancy-silicon complex

Phys. Rev. Lett., 77 (1996), pp. 3041-3044

[15] A.M. Zaitsev, V.S. Vavilov, A.A. Gippius

Cathodoluminescence of diamond associated with silicon impurity

Sov. Phys. Leb. Inst. Rep., 10 (1981), pp. 15-17

[16] C.D. Clark, H. Kanda, I. Kiflawi, G. Sittas

Silicon defects in diamond

Phys. Rev. B, 51 (1995), pp. 16681-16688

[17] C. Wang, C. Kurtsiefer, H. Weinfurter, B. Burchard

Single photon emission from SiV centres in diamond produced by ion implantation

J. Phys. B At. Mol. Opt. Phys., 39 (2006), pp. 37-41

[18] I.I. Vlasov, A.A. Shiryaev, T. Rendler, S. Steinert, Sang-Yun Lee, D. Antonov, *et al.*

Molecular-sized fluorescent nanodiamonds

Nat. Nanotechnol., 9 (2014), pp. 54-58

[19] A.A. Bergman, A.M. Zaitsev, A.A. Gorokhovsky

Polarization of luminescence and site symmetry of the Xe center in diamond

J. Lumin, 125 (2007), pp. 92-96

[20] J.P. Goss, B.J. Coomer, R. Jones, T.D. Shaw, P.R. Briddon, M. Rayson, *et al.*

Self-interstitial aggregation in diamond

Phys. Rev. B, 63 (2001), p. 195208

[21] J.P. Goss, B.J. Coomer, R. Jones, C.J. Fall, P.R. Briddon

Extended defects in diamond: the interstitial platelet

Phys. Rev. B, 67 (2003), p. 165208

[22] K.K. Ashikkalieva, T.V. Kononenko, E.A. Obraztsova, E.V. Zavedeev, A.A. Khomich, E.E. Ashkinazi, *et al.*

Direct observation of graphenic nanostructures inside femtosecondlaser modified diamond

Carbon, 102 (2016), pp. 383-389

[23] P.R. Biddon, R. Jones

Theory of impurities in diamond

Phys. B, 185 (1993), pp. 179-189

[24] A.T. Collins

The colour of diamond and how it may be changed

J. Gemmol., 27 (6) (2001), pp. 1355-1565

[25] A.M. Zaitsev, W. Wang, K.S. Moe, P. Johnson

Spectroscopic studies of yellow nitrogen-doped CVD diamonds

Diam. Relat. Mater., 68 (2016), pp. 51-61

[26] A.T. Collins

Optical centres produced in diamond by radiation damage

New Diam. Front. C Tec., 17 (2) (2007), pp. 47-61

[27] A.T. Collins, G. Davies, G.S. Woods

Spectroscopic studies of the H1b and H1c absorption lines in irradiated, annealed type-Ia diamonds

J. Phys. C. Sol. St. Phys., 19 (1986), pp. 3933-3944

[28] T. Hainschwang, S. Karampelas, E. Fritsch, F. Notari

Luminescence spectroscopy and microscopy applied to study gem materials: a case study of C centre containing diamonds

Min. Petrol, 107 (2013), pp. 393-413

[29] S.A. Solin

Photoluminescence of natural type I and type IIb diamonds

Phys. Lett., 38A (1972), pp. 101-102

[30] A. Osvet, V. Palm, I. Sildos

Spectral hole burning and uniaxial stress study of radiation-induced defects in diamond

J. Appl. Phys., 79 (1996), pp. 8290-8293

[31] J.E. Lowther

Jahn-Teller coupling at ND1 and GR1 centres in diamond

J. Phys. C. Solid State Phys., 11 (1978), pp. L373-L375

[32] G. Davies, C. Foy

Jahn-Teller coupling at the neutral vacancy in diamond

J. Phys. C. Solid St. Phys., 13 (1980), pp. 2203-2213

[33] V. Hizhnyakov, H. Kaasik, I. Sildos

Zero-phonon lines: the effect of a strong softening of elastic springs in the excited state

Phys. St. Sol., 234 (2002), pp. 644-653

[34] T. Feng, B.D. Schwartz

Characteristics and origin of the 1.681 eV luminescence center in chemical-vapor-deposited diamond films

J. Appl. Phys., 73 (1993), pp. 1415-1425

[35] Shaoheng Cheng, Jie Song, Qiliang Wang, Junsong Liu, Hongdong Li, Baolin Zhang

Plasmon resonance enhanced temperature-dependent photoluminescence of Si-V centers in diamond

Appl. Phys. Lett., 107 (2015), p. 211905

[36] E. Neu, C. Hepp, M. Hauschild, S. Gsell, M. Fischer, H. Sternschulte, *et al.*

Low-temperature investigations of single silicon vacancy colour centres in diamond

New J. Phys., 15 (2013), p. 043005

[37] S. Stoupin, Y.V. Shvyd'ko

Ultraprecise studies of the thermal expansion coefficient of diamond using backscattering x-ray diffraction

Phys. Rev. B, 83 (2011), p. 104102

[38] G. Davies

The Jahn-Teller effect and vibronic coupling at deep levels in diamond

Rep. Prog. Phys., 44 (1981), pp. 787-830

[39] P. Humble

The structure and mechanism of formation of platelets in natural type Ia diamond

Proc. R. Soc. Lond. Ser. A, 381 (1982), pp. 65-81

[40] G. Davies, H. Smith, H. Kanda

Self-interstitial in diamond

Phys. Rev. B, 62 (2000), pp. 1528-1531

[41] H.E. Smith, G. Davies, M.E. Newton, H. Kanda

Structure of the self-interstitial in diamond

Phys. Rev. B, 69 (2004), p. 045203

[42] H.L. McMurry, A.W. Solbrig Jr., J.K. Boyter, C. Noble

The use of valence force potentials in calculating crystal vibrations

J. Phys. Chem. Sol., 28 (1967), pp. 2359-2368

[43] S.J. Breuer, P.R. Briddon

Ab-initio investigation of the native defects in diamond and self-diffusion

Phys. Rev. B, 51 (1995), pp. 6984-6994

[44] V. Jelic, F. Marsiglio

The double well potential in quantum mechanics: a simple, numerically exact formulation

Eur. J. Phys., 33 (2012), pp. 1651-1661